catalysts

MDPI

Article

Synthesis of Nano-ZnO/Diatomite Composite and Research on Photoelectric Application

Beibei Yang [1], Xuefei Liu [1], Zixu Ma [1], Qian Wang [2] and Junjiao Yang [1,2,*]

[1] College of Chemsity, Beijing University of Chemical Technology, Beijing 100029, China; yangbeibei8896@163.com (B.Y.); liuxf0116@163.com (X.L.); 2019210576@mail.buct.edu.cn (Z.M.)
[2] Analysis and Test Center of Beijing University of Chemical Technology, Beijing University of Chemical Technology, Beijing 100029, China; wqian@mail.buct.edu.cn
* Correspondence: yangjj@mail.buct.edu.cn

Abstract: The key to the commercialization of sustainable energy conversion technologies is the development of high-performance catalysts. The discovery of a stable, efficient, and low-cost multi-function catalyst is key. We used a simple green precipitation method to load diatomite nanozinc oxide particles onto a diatomite substrate. The ZnO is nano-sized. This precipitation method produces ZnO nanoparticles in situ on diatomite. The catalyst degraded 90% of a Methylene blue solution and also degraded gaseous benzene and acetone. Not only can the catalyst be used for the organic degradation of wastewater, but it also has the potential to degrade volatile organic compounds. Photocatalytic efficiency is closely related to the generation and separation of photosynthetic electrons and holes. The effective suppression of the composite rate of photoliving carriers, and thus improvement of the photocatalytic activity, has become a key research area. At present, At present, photocatalysis is an effective technology to inhibit photocarrier synthesis, which is often studied in sewage treatment. Photocatalytic water treatment reduces the combination of photoelectrons and holes by applying an external bias, thus improving the quantum efficiency for the complete mineralization of organic pollutants. The composite catalyst was used for oxygen and hydrogen extraction reactions, and a comparison of the catalysts with various loading ratios showed that the electrolysis water activity of the in situ loaded catalyst is due to pure ZnO, and the efficiency is highest when the loading ratio is 10%. This work provides new methods for the design and further optimization of the preparation of electrolytic aqueous catalysts.

Keywords: photoelectric; ZnO nanoparticles; sewage treatment; volatile organic compounds; semiconductor; water splitting

Citation: Yang, B.; Liu, X.; Ma, Z.; Wang, Q.; Yang, J. Synthesis of Nano-ZnO/Diatomite Composite and Research on Photoelectric Application. *Catalysts* **2021**, *11*, 1232. https://doi.org/10.3390/catal11101232

Academic Editors: Wonyong Choi, Detlef W. Bahnemann, Ioannis Konstantinou, Ewa Kowalska, Magdalena Janus, Vincenzo Vaiano and Zhi Jiang

Received: 6 September 2021
Accepted: 11 October 2021
Published: 13 October 2021

1. Introduction

Photocatalytic technology is now considered the most promising technology for addressing energy shortages and environmental pollution. TiO_2 and ZnO are important semiconductor materials that are widely used in fields such as solar cells [1,2], photocatalysis [3], and environmental restoration. However, photocatalysts have low solar utilization and poor photoelectron and hole stability [4].

ZnO is a common semiconductor material with a band gap width of approximately 3.1~3.2 eV, with visible light response properties and appropriate valence and guide band positions, possessing strong oxidation-reduction capability. Extensive studies have shown that ZnO is a photocatalyst with excellent activities such as photocatalytic decomposition of water and degradation of organic pollutants under visible light [5]. Although ZnO has a suitable band gap, powder nanometer ZnO particles are small, and industrial use will cause harm to the human respiratory tract; nevertheless, it is an effective way to load nano ZnO to a larger substrate material from the perspective of increased use [6]. In addition, in terms of increasing the photocatalytic efficiency, ZnO can

be modified with alterations, including appearance regulation [7], element doping [8], crystal surface regulation [9], and the construction of heterojunctions [10–12]. It was shown that an oxygen vacancy, such as a crystal defect, can introduce new Fermi levels into a photocatalyst, increase the density of the photoraw carrier, promote the separation of the photoraw carrier, broaden the range of the visible light response, and significantly improve the performance of the photocatalyst [13].

In this study, ZnO composites with various loading ratios were synthesized by a precipitation method using diatomite as the carrier. Diatomite has the advantages of a large surface area, the presence of many voids, and a surface containing a great number of hydroxy groups [14,15]. Photocatalytic materials were analyzed by X-ray diffraction (XRD), scanning electron microscopy (SEM), and high-resolution transmission electron microscopy (HRTEM). Methylene blue (MB) was chosen as the target pollutant to investigate the effect of oxygen vacancy concentration on the degradation performance of the photocatalyst [16,17].

2. Results and Discussion

2.1. Phase Analysis

Figure 1 shows the XRD patterns of pure diatomite, pure ZnO, and X% ZnO@diatomite. The diffraction peaks at 31.8°, 34.4°, 36.2°, 47.5°, 56.6°, 62.8°, and 67.9° correspond to the crystal faces (100), (002), (101), (102), (110), (103), and (112) of hexagonal wurtzite ZnO, respectively [18,19]. The peaks at 21.8° and 36.5° are attributed to the SiO2 features in diatomite. All of the catalysts with various loading ratios show the coexistence of an anatase phase with no additional peak, implying that no impurity appears in ZnO when ZnO is supported on diatomite. The reflection peak of diatomite becomes relatively low compared with that of ZnO, and the pure diatomite peak is not too weak. Therefore, the introduction of diatomite does not affect the crystal structure of the catalyst. This result is consistent with the SEM and HRTEM characterizations.

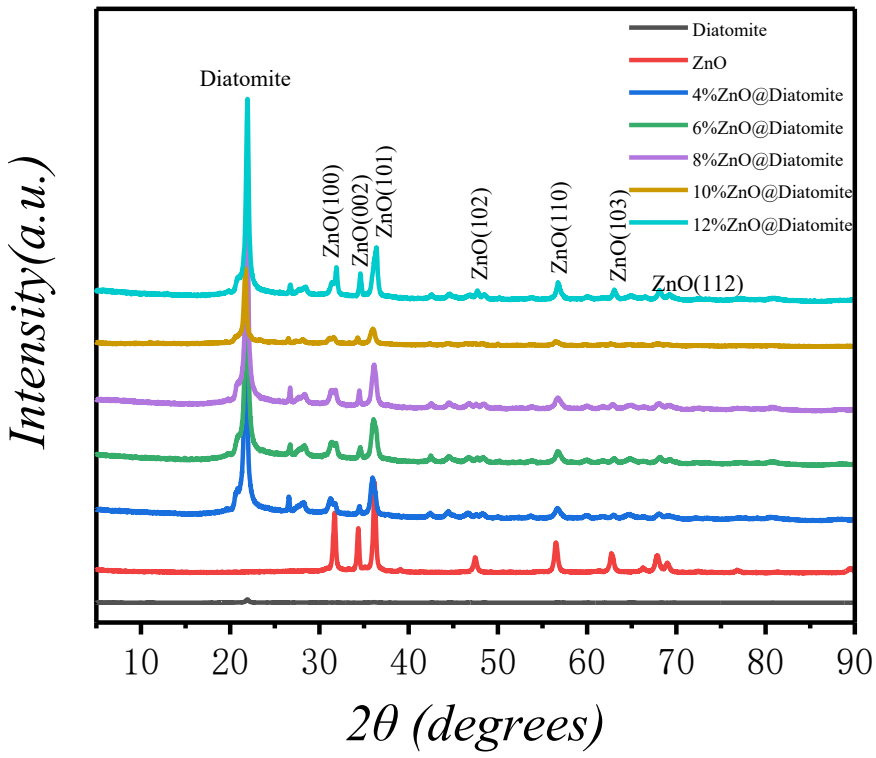

Figure 1. XRD patterns of pure diatomite, pure ZnO, and X% ZnO@diatomite.

2.2. SEM and HRTEM Investigations

The appearance of the catalyst was characterized by SEM and HRTEM, as shown in Figure 2. It can be seen in Figure 2(A1,A2) that pure diatomite without the loading of ZnO nanoparticles has the appearance of a sunflower, with a smooth surface and numerous pores. The SEM images of pure ZnO displayed in Figure 2(B1,B2) indicate that the ZnO nanoparticles are prism-like, and the diameter of the pure ZnO particles measure approximately 45 nm in size, corresponding to the results of UV diffuse calculations. As is shown in the SEM images, ZnO with molar ratio loads of 10% Figure 2(C1,C2) on diatomite has a size of approximately 15–20 nm. As shown in the HRTEM image in Figure 2(D1,D2), the lattice distance of ZnO is approximately 0.2488 nm, corresponding to the (101) plane of anatase ZnO.

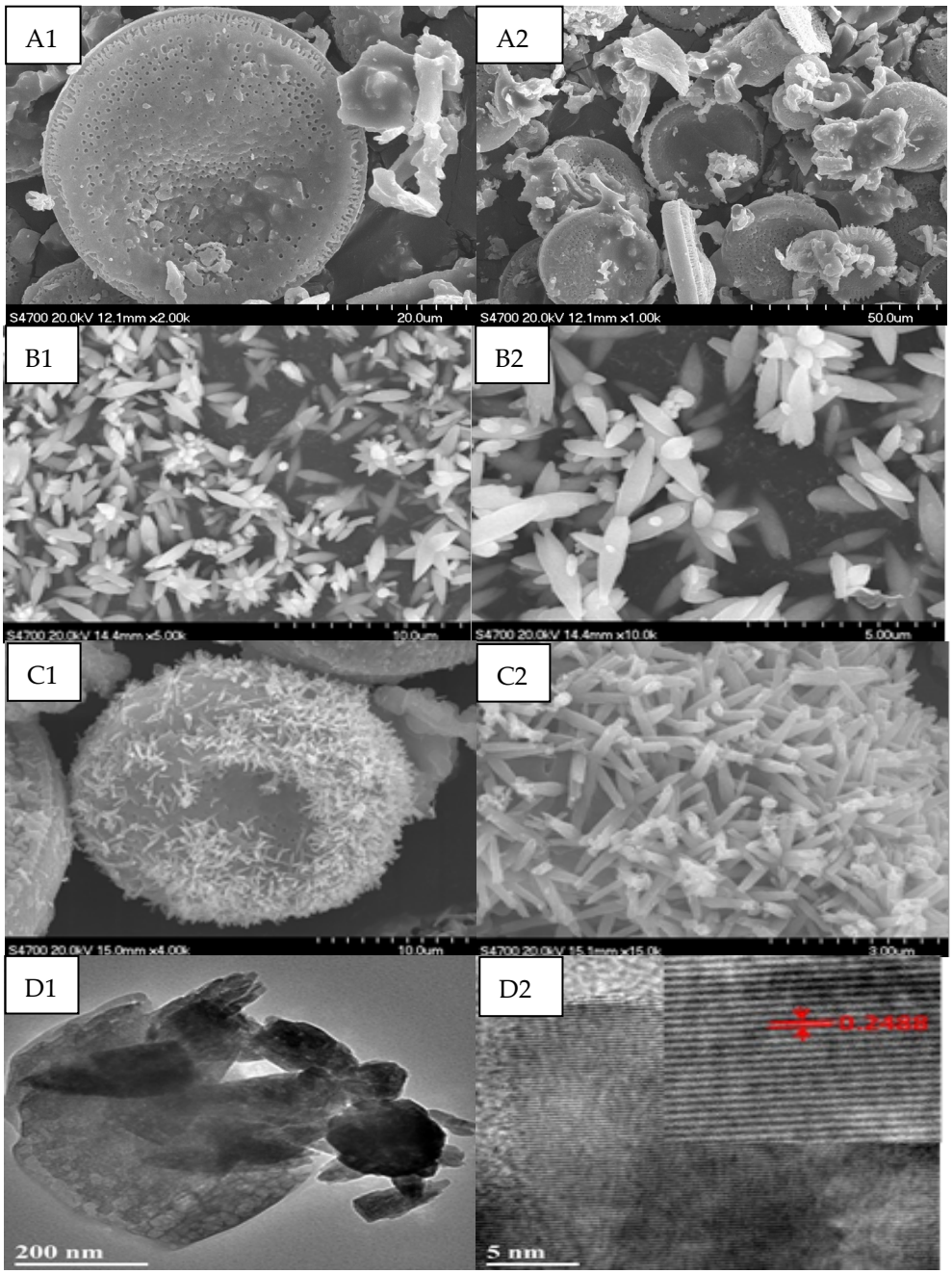

Figure 2. SEM images with different magnifications of (**A1**,**A2**) diatomite, (**B1**,**B2**) ZnO, and (**C1**,**C2**) 10% ZnO@diatomite; (**D1**,**D2**) HRTEM images of 10% ZnO@diatomite.

2.3. EDS Analysis

Figure 3 shows a diagram of the energy dispersive spectroscopy (EDS) and elemental mapping of the 10% ZnO@diatomite sample, which clearly shows that ZnO is uniformly distributed on the diatomite surface of silicon, and the Zn, O, and Si elements are evenly distributed.

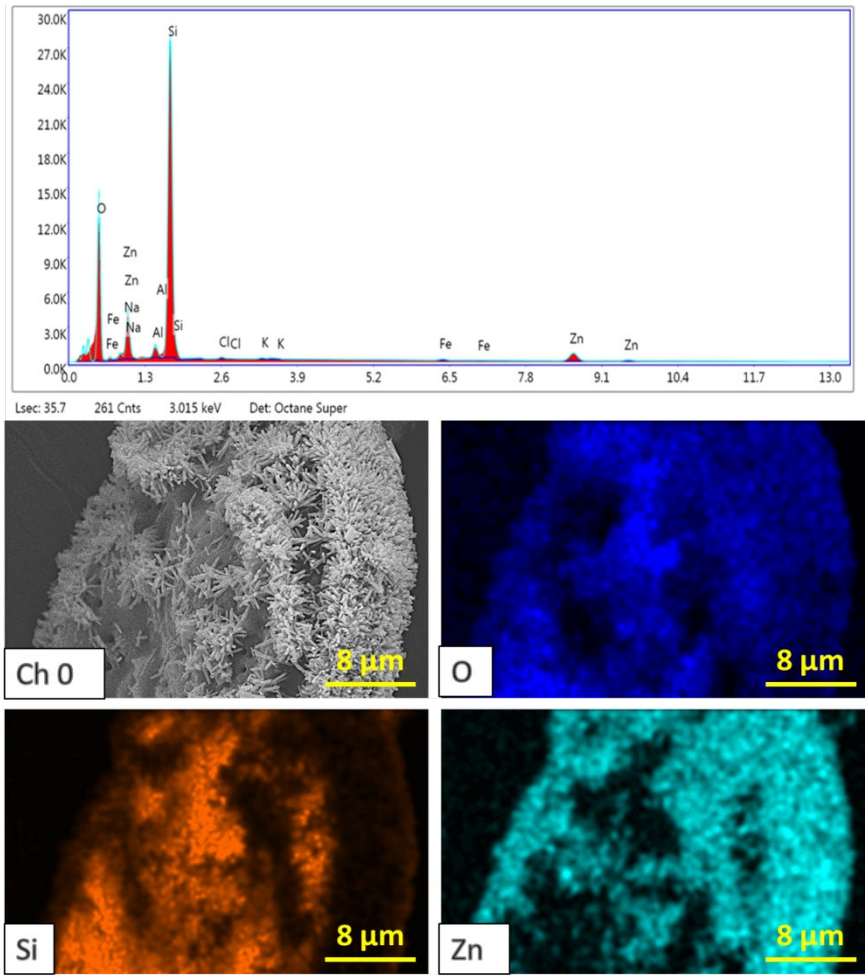

Figure 3. EDS and corresponding elemental mapping of 10% ZnO@diatomite.

2.4. EPR Analysis

For the photodegradation of organic dyes, three main active substances participate in the reaction, i.e., photoliving holes (h^+), hydroxyl radicals (·OH), and hyperoxygen radicals ($\cdot 0_2^-$) [20,21]. In order to explore the mechanisms of this photocatalytic process, triethanolamine (TEOA), isopropanol (IPA), and ascorbic acid (VC) were used to capture h^+, OH, and O^{-2} active species with capture amounts of 1 mmol, and the results are shown in Figure 4h. Figure 4h shows that the degradation rate of MB solution without any capture agent was 88.28% under visible light, while the degradation rate of the experimental group with the capture agent decreased to different degrees, with TEOA at 83.73%, IPA at 34.96%, and VC at 39.71%, respectively. This result shows that the influence of active species on photocatalytic MB solution is in the order of $h^+ < \cdot 0_2^- <$ ·OH. The photocatalytic properties of the material are closely related to the number of active species produced in the reaction system, so the electron paramagnetic resonance(EPR) technique was used to characterize the active species h^+, ·OH, and $\cdot 0_2^-$. Figure 4a–g shows the signals from active species h^+, ·OH, and $\cdot 0_2^-$. All the active species can be detected after irradiation with a xenon lamp, and the signal intensity of both active spe-

cies increases as the time of xenon lamp exposure increases. In Figure 4a–c, the samples were irradiated with the xenon lamp for 4 min or 8 min, and pure ZnO nanoparticles had the strongest signal of ·OH. In Figure 4d–f, the samples were irradiated with the xenon lamp for 4 min or 8 min, and 10% ZnO@diatomite had the strongest signal of $\cdot O_2^-$. In Figure 4g, the oxygen vacancy defect test results showed the largest number of oxygen vacancy defects in 10% ZnO@diatomite, indicating that the energy of the photocatalytic degradation of the MB solution is more closely related to $\cdot O_2^-$ and oxygen vacancies.

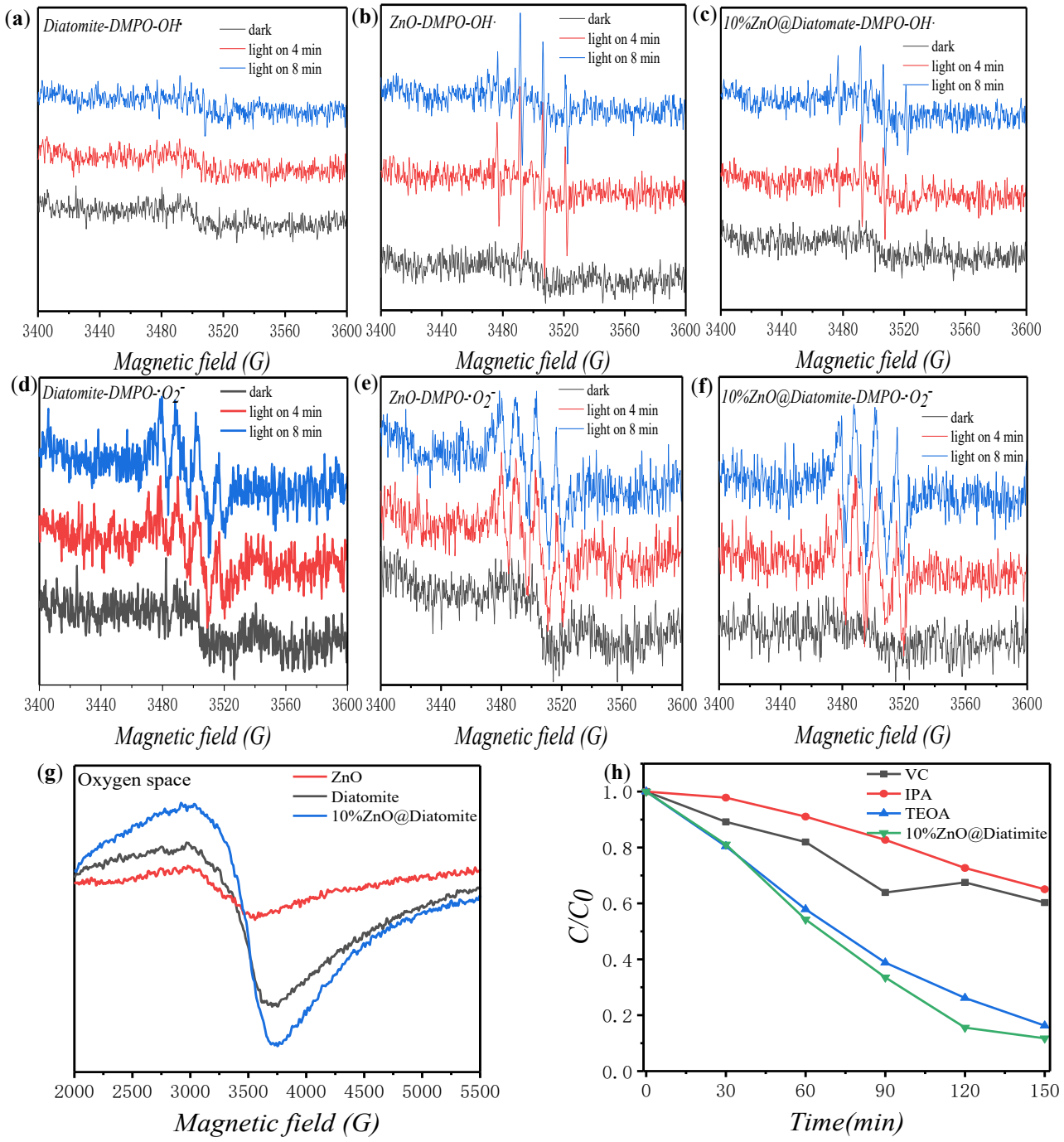

Figure 4. EPR spectra of the samples: (**a**)·OH in diatomite; (**b**)·OH in pure ZnO; (**c**)·OH in 10%ZnO@diatomite; (**d**) O^{-2} in diatomite; (**e**)·O^{-2} in pure ZnO; (**f**)·O^{-2} in 10%ZnO@diatomite; (**g**) oxygen vacancy; (**h**) degradation rate of MB solution by 10%ZnO@diatomite with the addition of various free radicals.

2.5. XPS Analysis

X-ray photoelectron spectroscopy (XPS) was conducted to analyze the elemental chemical environment [22,23]. Figure 5 shows the XPS results for pure ZnO and the composite catalyst with a loading ratio of 10%. The survey spectra of the two catalysts are shown in Figure 5a, where only the three elements Zn, O, and C are displayed for pure ZnO, and the four elements Si, Zn, O, and C are shown for the composite catalyst with a loading ratio of 10%. Figure 5b shows the 2p peak of Si (102.93 eV) for diatomite. The Zn 2p spectrum for pure ZnO (Figure 5c) shows a pair of peaks, at 1021.91 eV ($2p_{3/2}$) and 1044.79 eV ($2p_{1/2}$). The Zn 2p spectrum of composite catalysts (Figure 5c) shows a pair of peaks at 1022.23 eV ($2p_{3/2}$) and 1044.75 eV ($2p_{1/2}$). The results demonstrate that the ZnO interacts with the diatomite and generates a Zn–O–Si bond. Figure 5d is the O_{1s} for the two catalysts; generally, O_{1s} is divided into surface adsorption oxygen, metal–oxygen bonds, and oxygen vacancies. O_1 indicates metal–oxygen, O_2 is surface oxygen, and O_3 is oxygen vacancies. After comparative analysis, as shown in Table 1, the results show that O_1 and O_2 decreased slightly, while O_3 increased significantly. The presence of oxygen vacancies in the composite catalyst improves photocatalytic performance.

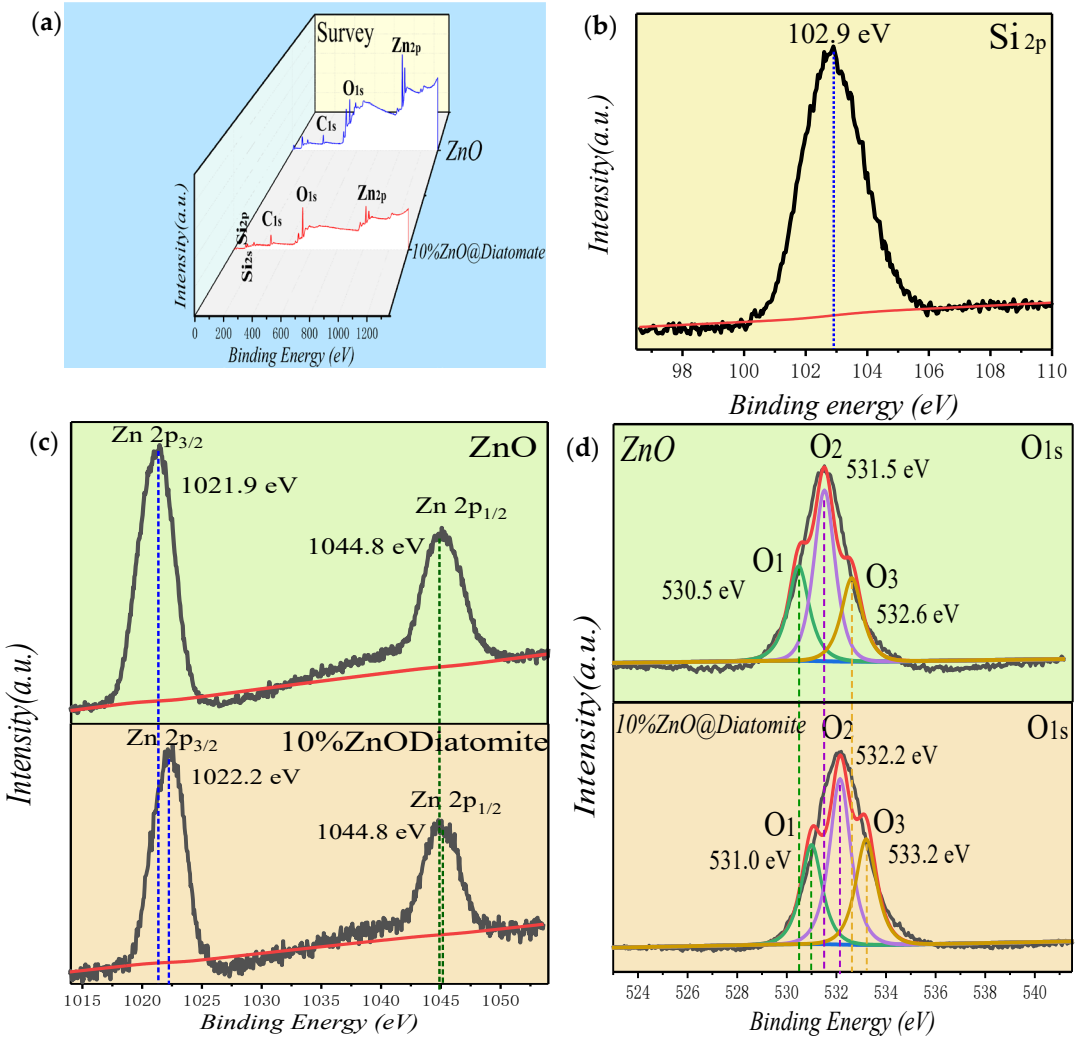

Figure 5. XPS survey spectra (**a**) and Si 2p (**b**), Zn 2p (**c**), and O 1s (**d**) spectra for ZnO and 10% ZnO@diatomite.

Table 1. Ratio of three binding energy levels of ZnO and 10% ZnO@diatomite.

Oxygen Species / Sample	O_1	O_2	O_3
ZnO	28.02%	47.81%	24.17%
10%ZnO@diatomite	26.77%	44.67%	28.56%

2.6. BET Analysis

The specific surface area and aperture size of the catalysts with various molar loading ratios were analyzed by Brunauer–Emmett–Teller (BET) testing, as shown in Table 2. The pure ZnO nanoparticles have the largest specific surface area, at approximately 65.65 m^2/g . However, the specific surface area and pore volume of pure diatomite is quite small; thus, the diatomite contributes less to the specific surface area of the X% ZnO@diatomite composites. The specific surface area and pore volume of the X% ZnO@diatomite composites are less than those of the pure ZnO nanoparticles. These results demonstrate that specific surface area and aperture size have little relationship with photocatalytic capacity. As can be seen from Figure 6, the diatomite shows International Union of Pure and Applied Chemistry (IUPAC) type-II isotherms, indicating the presence of micropores in the diatomite; the X% ZnO@diatomite composites display type-IV isotherms with an overlap of the H2 and H3 hysteresis loops, which is related to the deposition of ZnO nanoparticles on the surface of the diatomite.

Table 2. Surface and structural characterization of the catalysts.

Sample	BET Specific Surface Area (m^2/g)
Diatomite	1.19
4% ZnO@diatomite	1.38
6% ZnO@diatomite	2.15
10% ZnO@diatomite	2.52

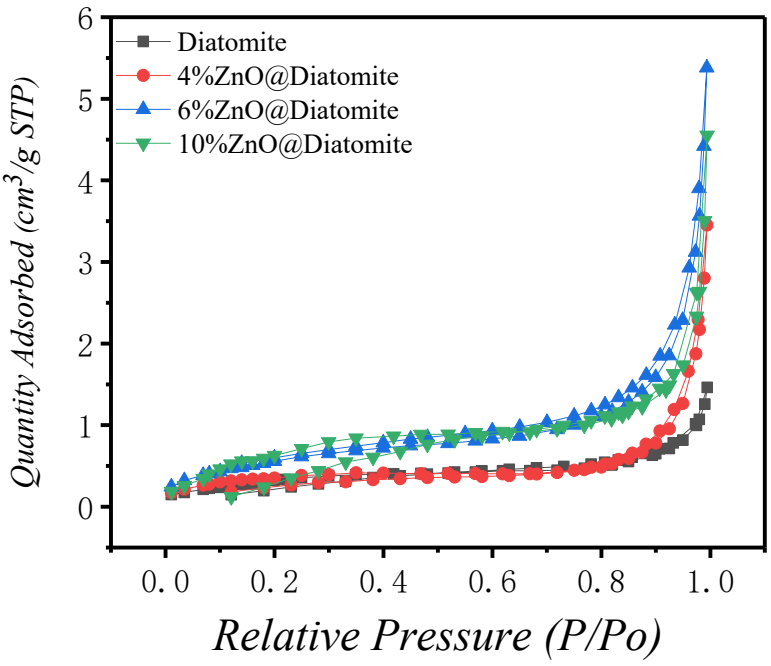

Figure 6. N_2 adsorption-desorption isotherms of diatomite, ZnO, and X% ZnO@diatomite composites.

2.7. UV-Vis Diffuse Reflectance Spectra

The absorption spectra of the samples were acquired using a UV visible spectroluminometer (UV-vis) with a wavelength scanning range of 200~800 nm, characterizing the optical absorption characteristics of the catalysts [24]. From Figure 7a, nano ZnO has a distinct UV absorption peak at 376 nm. However, for diatomite, there is no absorption above 400 nm. For the catalysts with various molar loading ratios, there are obvious UV absorption peaks at 376 nm, which proves the successful loading of ZnO. The analytical data show that the composites with various molar loading ratios had strong ultraviolet absorption at 10%. By using the Tauc plot, the band gaps of the samples were calculated. The broadening of the energy spacing of nanomaterials shows the size and the range of momentum and energy changes in electrons.

The optical absorption coefficient satisfies the equation:$\alpha^2 = (A/h\nu)(h\nu - Eg)$, α is the optical absorption coefficient, A is the proportional constant, h is the Planck constant , ν is the frequency of light, hν is the photon energy, Eg is the energy gap . The value of Eg is obtained by extending the linear part of the curve when α= 0. Figure 7b shows the $(\alpha h\nu)^2$–(hν) relationship curve of pure ZnO and 10% ZnO@diatomite, from which the band gap values are determined to be 3.26 eV and 3.33 eV, respectively. Figure 7c,d shows the XPS valence band spectra of pure ZnO and 10% ZnO@diatomite, determining that the valence bands are located at 2.47 eV and 3.09 eV, respectively. By combining the band gap values and valence value of the samples, the guide band bases of pure ZnO and 10% ZnO@diatomite are found at -0.79 eV and -0.24 eV, respectively. It was reported in the literature that (H_2O /·OH) has a redox potential of 2.38 eV, while the (0_2/· 0_2^-) redox potential is -0.33 eV. Obviously, the calculated energy band structures for the samples conform to the excitation of solar lamps (·OH) and the formation of potential requirements for · 0_2^- active species.

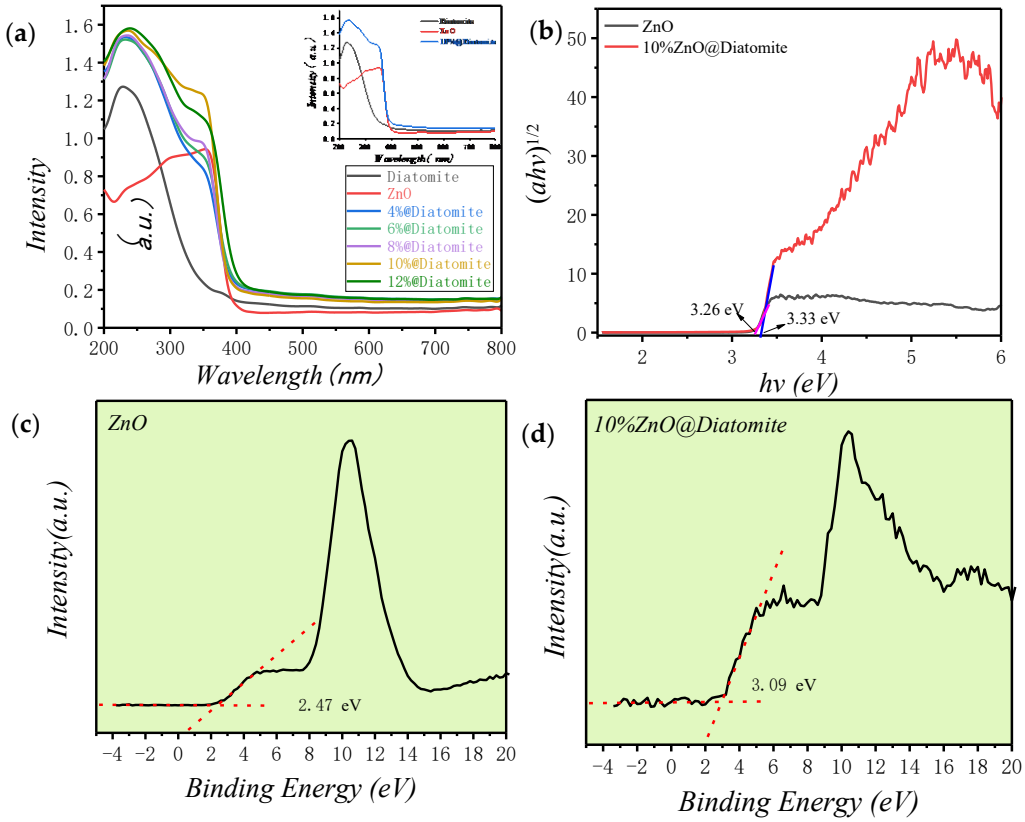

Figure 7. (**a**)UV-vis spectra of X% ZnO@diatomite, (**b**)plots of $(\alpha h\nu)^2$ versus (hν), (**c**)XPS valence band spectra of pure ZnO, (**d**)XPS valence band spectra of pure ZnO.

2.8. Photoluminescence (PL) Spectra

The (PL) spectra of the prepared samples are shown in Figure 8. Because the majority of optical absorption and subsequent photoexcitation takes place within the surface region of the photocatalyst, the emission mostly reflects the surface charge recombination [25]. One of the important evaluation criteria for photocatalytic capacity is the composite rate of electrons and holes, and as the composite rate decreases, the photocatalytic capacity of the catalyst grows stronger [26,27]. The wavelength of the excitation light selected in the experiment was 300 nm. The obtained test results are shown in Figure 8. After the ZnO was loaded on diatomite, the fluorescence intensity was lower than that of the pure diatomite or ZnO, and the fluorescence intensity for the composite with the molar loading ratio of 10% was the lowest, and the photocatalytic performance was the best. The weakening in fluorescence intensity may be due to ZnO loading on diatomite; by forming Si–O–Zn, ZnO nanoparticles can act as good electron trackers, slowing the combination of electrons and holes. Therefore, we concluded that the catalyst with the ZnO molar loading ratio of 10% was the most suitable for the photocatalytic degradation experiment.

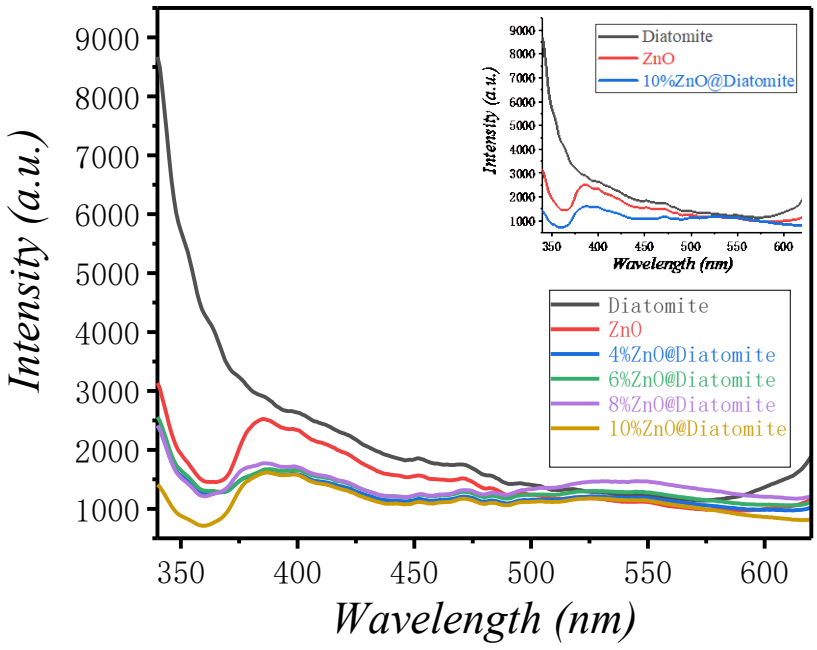

Figure 8. PL spectra of ZnO, diatomite, and X% ZnO@diatomite.

2.9. Photocatalytic Performance of Catalysts

Semiconductor photocatalytic technology is a catalytic oxidation technology that has received much research attention. Photocatalytic technology is a heterogeneous photocatalytic process under light irradiation, making it an ideal photocatalytic process to use sunlight as a light source and activate the oxidation-reduction reaction at room temperature [28–30]. Free radicals such as ·OH and $\cdot 0_2^-$ generated during the reaction are highly oxidizing, so they can effectively break the chemical bonds in organic compounds, thus achieving the photocatalytic oxidation and decomposition of polluted wastewater, organic polluting substances, or harmful gases on the surface of objects. Scheme 1 illustrates the formation of ZnO@diatomite hybrids, and the reaction process of the photocatalytic oxidation of pollutants such as MB is shown in Figure 9. The reaction expression is as follows:

$$ZnO + h\nu \rightarrow h^+ + e^-;$$

$$H_2O+h^+ \rightarrow \cdot OH + H^+;$$

$$O_2+e^- \rightarrow \cdot O_2^-;$$

$$\cdot OH + MB \rightarrow H_2O+CO_2;$$

$$\cdot O_2^- + MB \rightarrow H_2O+CO_2;$$

$$H^+ + \cdot O_2^- \rightarrow \cdot OOH;$$

$$\cdot OOH + \cdot OOH \rightarrow O_2 + H_2O_2;$$

$$H_2O_2+e^- \rightarrow 0H^- + \cdot OH;$$

$$\cdot OH, \cdot O_2^-;\ h^+ + MB \rightarrow H_2O+CO_2+\text{inorganic molecules.}$$

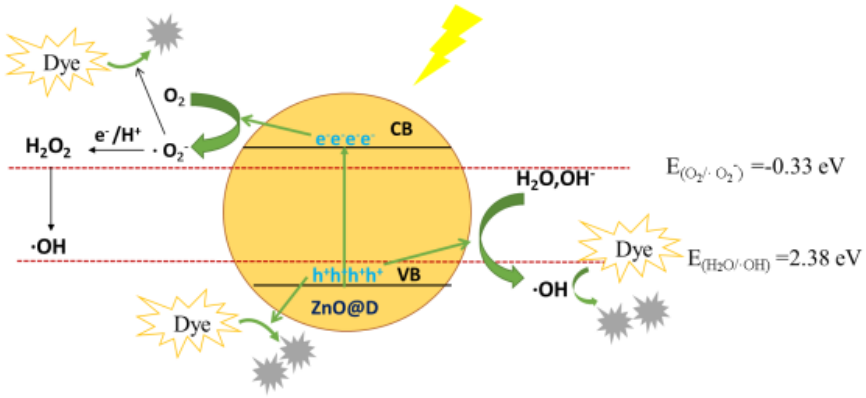

Figure 9. Schematic drawing of photocatalytic mechanism of ZnO@diatomite.

Scheme 1. Schematic illustration of the formation of ZnO@diatomite hybrids.

MB solution was used as the target degradator to evaluate the photocatalytic degradation ability of the catalyst with various molar loading ratios. By analyzing the specific surface area of the catalyst with various loading ratios, considering the strong adsorption capacity for MB solution under the condition of a low load, the optical absorption range was obtained by UV-vis spectroscopy, and the electron-hole composite rate was determined by PL spectroscopy. The catalyst with a molar loading ratio of 10% had the best photocatalytic degradation efficiency, as shown in Figures 10 and 11. At the same degradation time, the catalyst degradation efficiency of the composite with a molar loading ratio of 10% reached 90%, better than the catalysts with other loading ratios. The MB solution showed nearly no degradation with only diatomite. All the results are consistent with the UV and fluorescence analysis conclusions. The optimal value of the load may be due to the aggregation of ZnO nanoparticles and the saturation of the number of

Si–O–Zn bonds formed between diatomite and ZnO, resulting in a lower degradation efficiency when the load was 12% compared with that when the loading ratio was 10%.

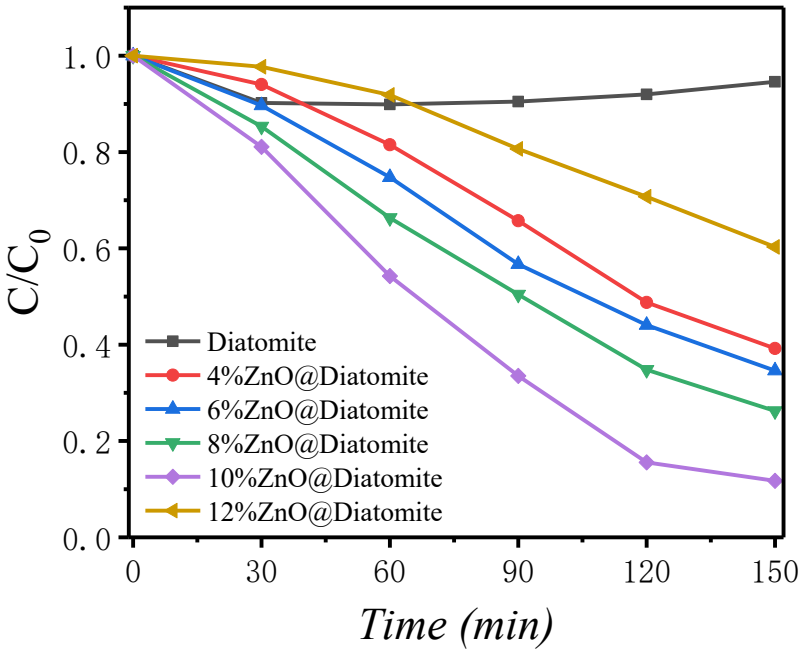

Figure 10. MB photodegradation over various catalysts under visible light.

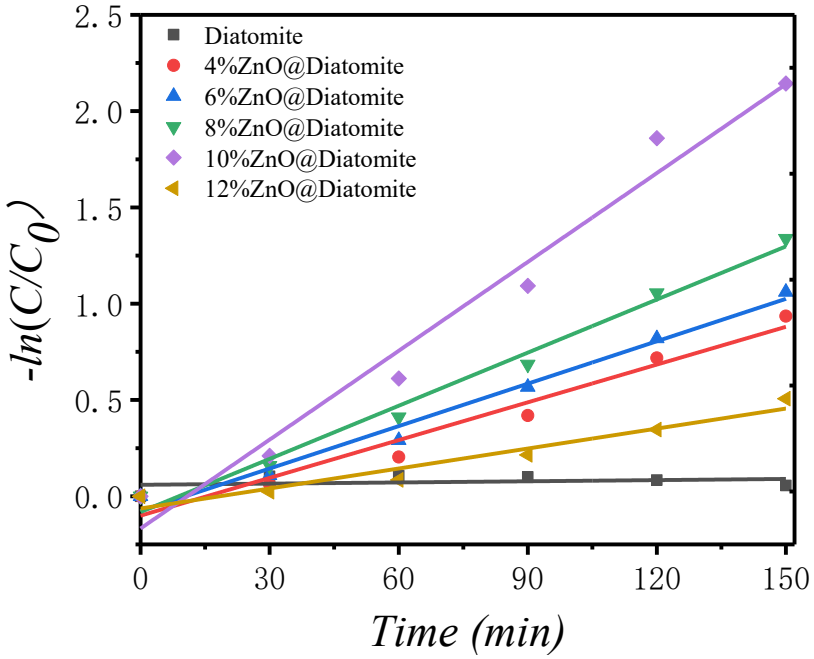

Figure 11. Primary kinetics fitting curve for photocatalytic degradation of MB.

Figure 12 shows the degradation results for gaseous acetone and gaseous benzene. The gas concentration was controlled by adding 1 mL of saturated gas at room temperature to headspace vials. As can be seen from Figure 12, under visible light irradiation, the optimal catalyst showed excellent photocatalytic performance for gaseous acetone and gaseous benzene at a certain concentration condition. As shown, both gaseous benzene and gaseous acetone degraded significantly after 180 min of light exposure, with gaseous acetone having higher degradation efficiency than that of gaseous benzene, but both showed incomplete degradation in a short amount of time because the initial con-

centration was too high. One of the possible reasons for the analytical degradation results is that the structure of the benzene molecules is extremely stable and difficult to break. Another possible reason is that the gaseous benzene concentration is too high or that it is non-polar, and the degradation efficiency may be related to molecular polarity. In this study, only two gaseous organic pollutants were studied. In the future, we will study the catalytic degradation of other gaseous organic pollutants (such as methanol, ethanol and formaldehyde) and determine whether the effects on polar organic and non-polar organic properties are the same.

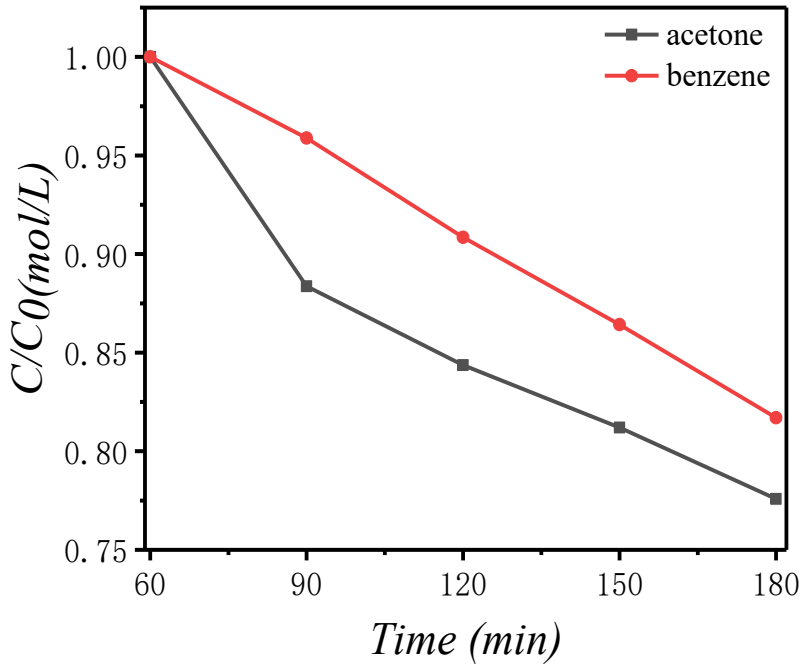

Figure 12. Photodegradation of certain concentrations of gaseous acetone and gaseous benzene over 10% ZnO@diatomite under visible light irradiation.

2.10. Photocurrent Analysis

Figure 13a shows a photoflow response curve of a photocatalyst with pure ZnO and composites with various molar loading ratios. The photoresponse current density of the ZnO @diatomite complex is greater than that of pure ZnO, and the catalyst photocurrent density with a molar loading ratio of 10% is the largest, indicating that the existence of oxygen vacancies can improve the separation efficiency of the sample photoelectron and hole, as with more oxygen vacancies, the improvement efficiency increases.

The composites with various loading ratios were studied to determine the maximum optical current density, as shown in Figure 13b. The comparison between dark and light conditions reveals that the optical current density in light conditions is significantly greater than that in dark conditions. Among them, the maximum optical current density of the composite with a loading ratio of 10% was 0.25 mA/cm^2 at + 0.8 V vs. Reversible Hydrogen Electrode (RHE). The composite has a high density, a high surface area, a high volume ratio, and a superior charge transport path, maximizing the optical current density. It is shown that 10%ZnO@diatomite has the largest photocurrent among the composite catalysts because of its charge collection efficiency and direct path to photoelectrons.

In this study, the ZnO@diatomite complex generates Zn–O–Si bonds with similar heterogeneous structures, thus improving the Passivated Emitterand Rear Cell (PEC) performance of ZnO nanoparticles. The ZnO@diatomite complex structure exhibits a higher absorbance in the UV-vis region compared with that of pure ZnO nanoparticles. Furthermore, the ZnO@diatomite has a smaller diameter and length compared with pure

ZnO nanoparticles, providing a higher surface–volume ratio for the electrode/electrolyte interface. Thus, as the Fermi level changes because of the strong interface interaction, more electron-hole pairs are produced, which are effectively separated. Furthermore, ZnO nanoparticles with smaller particle sizes on the complex are more prone to adsorption and surface reaction, thus further promoting charge separation. Additionally, the electrons and holes on the surface of ZnO nanoparticles were significantly reduced, as demonstrated by PL results. Therefore, the effective separation and transport of composite carriers, compared with the absorption of light, is often considered the main factor that determines the performance of PEC [17].

In the case of a low ZnO loading ratio, the electrolyte may directly meet the diatomite because of the small and uneven amounts of ZnO, which hinders the separation of photoraw charges with low photocurrent density. For the composite with a loading ratio of 10%, the maximum optical current density is due to the optimal ratio, leading to the effective separation of the photoraw carriers. When the load fraction is too high, ZnO nanoparticles can agglomerate, causing reduced photoraw carrier separation. Conversely, with an increase in the ZnO load, the charge transfer path increases, leading to an increase in combination and reduced separation of the carriers, leading to a decrease in the optical current density. The optimum load of nanoparticles is important for increasing the optical current density.

Electrochemical impedance spectroscopy (EIS) results are shown in Figure 13c for pure ZnO nanoparticles and ZnO@diatomite composite electrodes, obtaining the light response, stability, and charge transfer characteristics at the electrode/electrolyte interface. Figure 13c shows the current versus time (I–t) curves of pure ZnO nanoparticles and X% ZnO@diatomite composites in truncated light with a +0.8 V vs. RHE ≥ 400 s, on/off cycle of 50 s. When the lamp was turned off, both optical anodes displayed a very low dark current of approximately 0.0075 mA/cm^2. Under the light, we observed distinct light response platforms with a large and smooth photoflow, indicating a rapid separation of photobiological electrons. Compared with that of the pure ZnO nanoparticles, the optical response currents of the composites were all higher. This result shows a fast light response and reproduces the same light response within 400 s. Furthermore, the electrode material without degradation was observed from the transparent electrolyte solution, suggesting that there may be no change in any structure or morphology in the electrode. Thus, these observations indicate the stability of the photoanode in the PEC process. The obtained fast light response and chemical stability can be attributed to the loading of ZnO, generating Zn–O–Si bonds, which allows photoraw electrons to separate quickly and efficiently. Figure 13d shows the efficiency diagrams of composites with various loading ratios for water electrolysis, where it is clear that the efficiency of the catalyst after loading is greater than that of pure ZnO nanoparticles, indicating that the Si–O–Zn bonds are conducive to the transmission of electrons and improve the efficiency of water electrolysis [31].

To summarize, a schematic of the X% ZnO@diatomite composite hydrolysis device is shown in Figure 13e, and the interface charge separation process and its energy band diagram are shown in Figure 13f. When the photoelectrode is illuminated, the photoraw electrons and holes separate as a result of the electric field. The photoelectrons generated by X% ZnO@diatomite under light conditions move to the Pt electrode via an external circuit. These photoraw electrons reduce water to hydrogen by reaction with hydrogen ions in the electrolyte. Meanwhile, the holes produced in the valence band will effectively transfer to the electrode surface through the valence band because of the action of the built-in electric field, where they participate in the oxidation of water. Thus, an enhanced photocurrent is observed with the X% ZnO@diatomite composite. The presence of the X% ZnO@diatomite composite improves the charge separation efficiency.

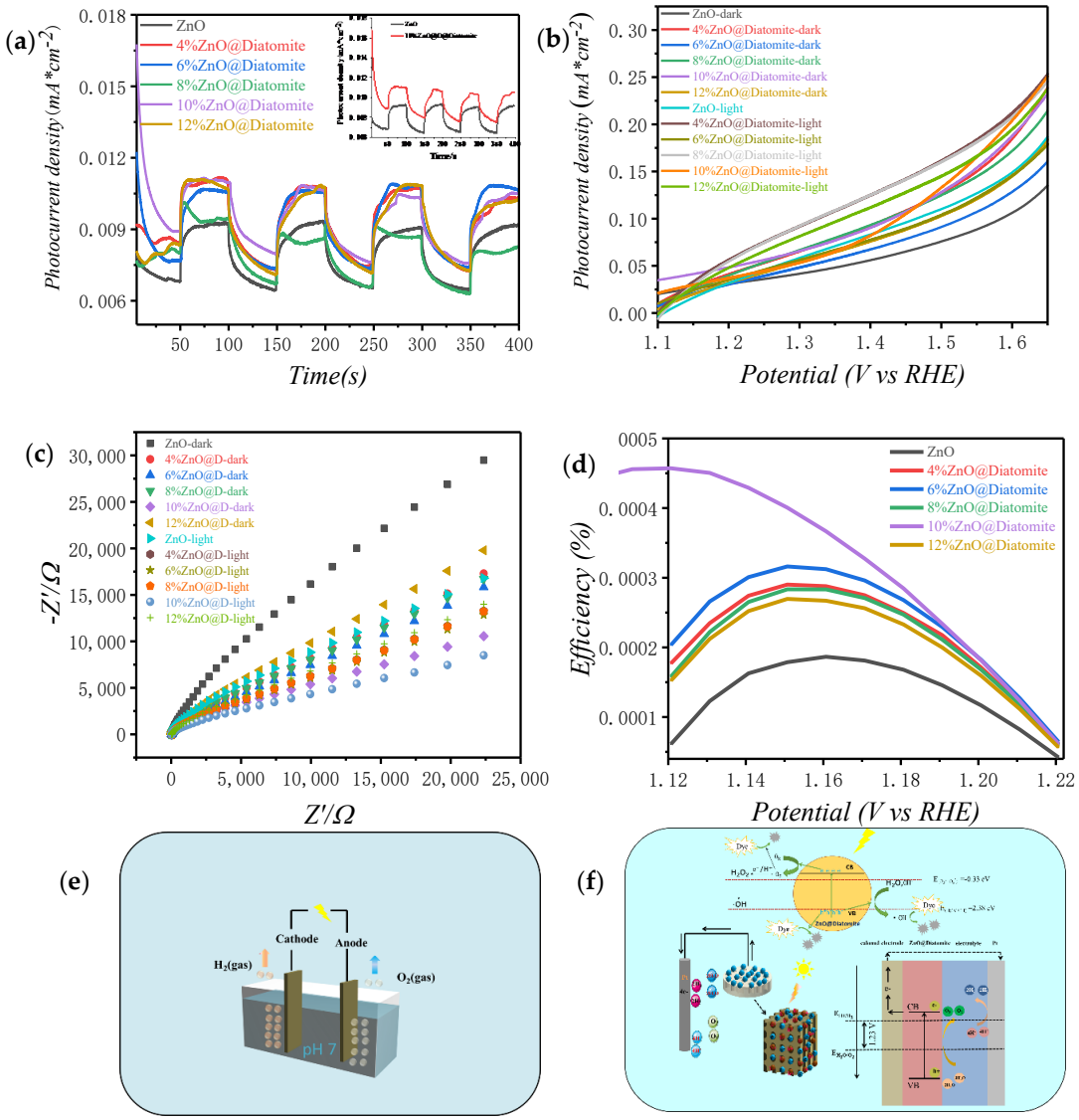

Figure 13. (**a**) Amperometric I–t curves. (**b**) Water splitting efficiency of pure ZnO and X% ZnO@diatomite. (**c**) Nyquist plots of pure ZnO and X%ZnO@diatomite. (**d**) Photocurrent density. (**e**,**f**) Schematic representation of the possible mechanism of photogenerated charge separation at the interface of X% ZnO@diatomite with the corresponding energy band diagram during PEC water splitting.

3. Experimental Section

3.1. Chemicals and Materials

Diatomite (Macklin, Shanghai, China), zinc acetate hexahydrate $Zn(OOCCH_3)_2{\cdot}2H_2O$ (Alfa Aesar, Shanghai, China), ammonia water (analytical reagent, Beijing, China), acetylacetone (analytical reagent, Tianjin, China), acetone (analytical reagent, Beijing, China), benzene(Aladdin, shanghai, China), TEOA (analytical reagent, Beijing, China), IPA (analytical reagent, Beijing, China), Nafion(Aladdin, shanghai, China), VC (Aladdin, shanghai, China), anhydrous ethanol (analytical reagent, Beijing, China) and deionized water were used for the synthesis of ZnO and ZnO/diatomite. During the process of synthesizing ZnO/diatomite, the molar ratio of ZnO to diatomite was controlled to synthesize composites with various load proportions. All the reagents listed were used as purchased and without further treatment.

3.2. Catalyst Preparation

First, a set mass of diatomite was weighed and placed in a 250-mL round-bottom flask; then, 40 mL of deionized water was added, and the mixture was stirred with the magnetic force for 30 min in an ice water bath. Second, $Zn(OOCCH_3)_2{\cdot}2H_2O$ was added and stirred for 30 min. Third, while stirring in an ice-water bath, 0.3% ammonia solution was added drop by drop into a three-neck flask, with a dropping speed of one drop per second. Then 2 mL of acetylacetone was added 10 min after the ammonia; when the pH value of the solution was 10.00, the dropping of the ammonia solution was stopped. This solution was heated in a water bath at 75 °C for 7 h. Finally, when the reaction was finished, the reacted mixed liquid in the round-bottom flask was washed with deionized water 3–5 times, washed to neutrality, and naturally dried for 5–15 h. Composites with various proportions of ZnO and diatomite were prepared by the same method, with loading ratios of 4%, 6%, 8%, 10%, and 12%. The pure ZnO was prepared according to the above procedure, except with the addition of diatomite steps. The preparation process is shown in Scheme 2.

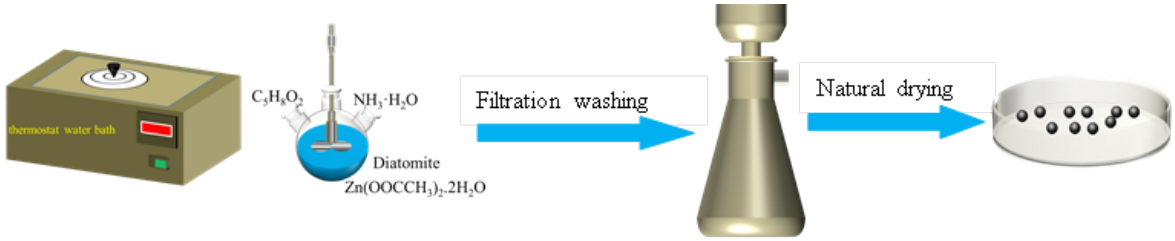

Scheme 2. Flow chart of photocatalyst preparation.

3.3. Characterization

3.3.1. Material Characterization

The surface morphology of samples was observed using SEM (JSM-7800F and S-4700, Japan) with EDS. The crystallinity of the prepared samples was characterized by XRD recorded using Cu Kα radiation at a scan rate of 5°/ min and HRTEM (ARM-200, Japan). The specific surface area and pore size distribution of the prepared samples were characterized by a BET instrument at 77 K (Micrometrics ASAP 2020, Georgia, USA). UV-vis absorbance was characterized using a UV-VISNIR spectrophotometer (SolidSpec-3700, Shimadzu, Japan). A photoluminescence spectrometer (FL-7000, Hitachi, Japan) was used out to evaluate the photocatalytic activity. XPS was conducted to analyze the elemental chemical environment. EPR (EMX-500 10/12) was used to detect unpaired electrons contained in atoms or molecules from qualitative and quantitative perspectives and to explore the structural properties of their surroundings. At room temperature, in 0.5 M Na_2SO_4 solution, a CHI660E electrochemical analyzer was used with a traditional three-electrode system. The prepared X% ZnO@diatomite catalyst was used as the working electrode, a glycerol electrode was the parameter electrode, and the pair electrode was composed of graphite.

3.3.2. Photocatalytic Activity

Samples with various loading ratios were evaluated using an MB solution photocatalytic degradation method. The analytical balance weighed 50 mg catalyst with a 30 mL concentration of 5 mg /L MB solution added to a 250 mL glass bottle, as shown in Scheme 3. The bottle was then placed in a heated xenon lamp box. First, static dark adsorption proceeds for 30 min in dark conditions, and then take 4 mL MB solution from the glass bottle into a sample tube measuring 5 mL and mark it as serial number 1. Turn on the xenon light and then take 4 mL MB solution from the glass bottle. The xenon lamp will always be illuminated. Then, 4 mL methylene blue solution is taken out every 30 min and marked as 3–6. The degradation rate was determined by monitoring the variation in

MB solution concentration over time using a UV-vis spectrophotometer (ShimUV-3600). The catalyst with the highest degradation rate was selected to degrade gaseous organic pollutants, including acetone and benzene. The degradation process was performed in headspace vials with a volume of 500 mL. Under sealed conditions, the saturated gas has the same concentration as the liquid. The specific experimental details are similar to those for the MB solution degradation process, but MB solution was replaced by gas-phase organic pollutants. The details of the experiment are as follows: the catalyst (0.05 g) was added to a headspace vials bottle, and 1 mL of the saturated gas pollutant was transferred to the headspace vials using a gas chromatographic syringe of 2.5 mL. A xenon lamp (30 W) was used as a light source during photocatalytic degradation. The headspace vials were placed in light, and the bottle was directly irradiated. The whole process was performed at room temperature. No heating or stirring was used throughout the degradation. Meanwhile, the gas was collected every 30 min, and the corresponding concentration of organic gas pollutants was determined by gas chromatography–mass spectrometry (GC–MS).

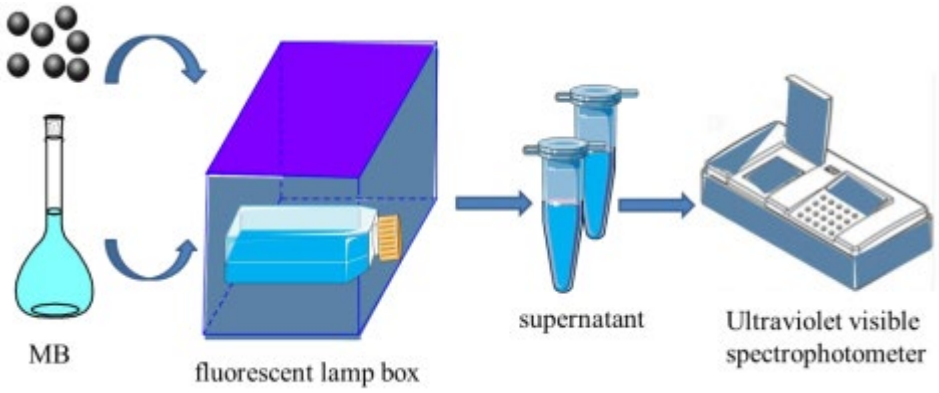

Scheme 3. Flow chart of photocatalyst degradation of MB.

3.3.3. Electrochemical Measurements of Electrocatalysts

Electrolysis water activity testing of the catalysts used a three-electrode system, including a working electrode, calomel electrode as the reference electrode, and a pair electrode composed of graphite. The 0.5 M Na_2SO_4 solution acted as an electrolyte solution, and the working electrode was prepared without any conductive substance. A total of 10 mg of catalyst was ultrasonically dispersed into a mixed solution of deionized water (475 μL) ,aqueous ethanol(475 μL) and Nafion solution(30 μL), where the pipettor took 5-μL droplets to the platinum carbon electrode as the working electrode, and the platinum carbon electrode area was 0.1256 cm^2. All electrodes were connected to an external circuit via a small crocodile needle. It was also ensured that there was no contact between the crocodile needle and the electrolyte. The photocurrent was measured under the irradiation of 150-mW/cm^2 xenon lamps. Linear scanning voltammetry (LSV) was performed at a rate of 10 mV/s between 0.4 and 1 V. Photochemical measurements were performed in both dark and simulated sunlight conditions. The efficiency of the decomposition of water was calculated using the following formula:

$$\eta(\%)=J\ (1.23-E_{RHE})/\ I_{light} \quad (1)$$

where η (%) is the efficiency of the decomposition of water, E_{RHE} is the potential calibrated against RHE and I_{light} is the optical current density.

4. Conclusions

X% ZnO@diatomite was successfully prepared by a precipitation method, and the diameter of the synthesized catalysts was 15–20 nm. The ZnO has nanoscale features and was relatively uniformly loaded on diatomite, solving the problem of limited utilization and recovery difficulty of nanomaterials. The catalyst was successfully prepared by the green pollution-free precipitation method. Under visible light irradiation, the optimal catalyst showed excellent photocatalytic performance for MB solution, gaseous acetone, and gaseous benzene. The experiments demonstrate that the catalyst has great potential for application to volatile organic compounds. By adjusting the loading ratio, the composite achieved high catalytic degradation, and the best degradation efficiency occurred at a molar loading ratio of 10%. At + 0.8 V vs. RHE, the maximum hydrocracking efficiency of the 10% ZnO@diatomite composite was 0.045%. XPS results proved the existence of Si–O–Zn bonds, providing a theoretical basis for the degradation mechanism. The results are consistent with conclusions reached from characterization techniques such as XRD and UV and fluorescence spectroscopy. The experimental catalyst not only can be conveniently recycled, but it also has great potential for the photocatalytic degradation of pollutants.

Author Contributions: Conceptualization, B.Y. and J.Y.; methodology, B.Y.; software, B.Y., X.L. and Q.W.; validation, B.Y., X.L. and Z.M.; formal analysis, B.Y.; investigation, B.Y.; resources, B.Y.; data curation, B.Y.; writing—original draft preparation, B.Y.; writing—review and editing, B.Y. and J.Y.; visualization, B.Y., J.Y. and X.L.; supervision, J.Y.; project administration, J.Y.; funding acquisition, J.Y. All authors have read and agreed to the published version of the manuscript.

Funding: This research received no external funding.

Data Availability Statement: The raw data supporting the conclusions of this article will be made available by the authors, without undue reservation.

Conflicts of Interest: The authors declare no conflict of interest.

References

1. Zhang, R.; Fei, C.; Li, B.; Fu, H.; Tian, J.; Cao, G. Continuous size tuning of monodispersed ZnO nanoparticles and its size effect on the performance of perovskite solar cells. *ACS Appl. Mater. Interfaces* **2017**, *9*, 9785–9794, https://doi.org/10.1021/acsami.7b00726.
2. Wang, D.; Zhou, Z.-H.; Yang, H.; Shen, K.-B.; Huang, Y.; Shen, S. Preparation of TiO_2 loaded with crystalline nano Ag by a one-step low-temperature hydrothermal method. *J. Mater. Chem.* **2012**, *22*, 16306–16311, https://doi.org/10.1039/c2jm16217b.
3. Sakthivel, S.; Neppolian, B.; Shankar, M.; Arabindoo, B.; Palanichamy, M.; Murugesan, V. Solar photocatalytic degradation of azo dye: comparison of photocatalytic efficiency of ZnO and TiO_2. *Sol. Energy Mater. Sol. Cells* **2003**, *77*, 65–82, https://doi.org/10.1016/s0927-0248(02)00255-6.
4. Kim, D.; Yong, K. Boron doping induced charge transfer switching of a C_3N_4/ZnO photocatalyst from Z-scheme to type II to enhance photocatalytic hydrogen production. *Appl. Catal. B Environ.* **2021**, *282*, 119538, https://doi.org/10.1016/j.apcatb.2020.119538.
5. Chankhanittha, T.; Nanan, S. Visible-light-driven photocatalytic degradation of ofloxacin (OFL) antibiotic and Rhodamine B (RhB) dye by solvothermally grown ZnO/Bi_2MoO_6 heterojunction. *J. Colloid Interface Sci.* **2020**, *582*, 412–427, https://doi.org/10.1016/j.jcis.2020.08.061.
6. Gupta, N.K.; Bae, J.; Kim, S.; Kim, K.S. Fabrication of Zn-MOF/ZnO nanocomposites for room temperature H2S removal: Adsorption, regeneration, and mechanism. *Chemosphere* **2021**, *274*, 129789.
7. Qian, C.; Yin, J.; Zhao, J.; Li, X.; Wang, S.; Bai, Z.; Jiao, T. Facile preparation and highly efficient photodegradation performances of self-assembled Artemia eggshell-ZnO nanocomposites for wastewater treatment. *Colloids Surf. A Physicochem. Eng. Aspects* **2021**, *610*, 125752.
8. Fernando, J.F.S.; Shortell, M.P.; Noble, C.J.; Harmer, J.R.; Jaatinen, E.A.; Waclawik, E.R. Controlling Au photodeposition on large ZnO nanoparticles. *ACS Appl. Mater. Interfaces* **2016**, *8*, 14271–14283, https://doi.org/10.1021/acsami.6b03128.
9. Hong, R.; Pan, T.; Qian, J.; Li, H. Synthesis and surface modification of ZnO nanoparticles. *Chem. Eng. J.* **2006**, *119*, 71–81, https://doi.org/10.1016/j.cej.2006.03.003.
10. Sernelius, B.; Berggren, K.-F.; Jin, Z.-C.; Hamberg, I.; Granqvist, C.G. Band-gap tailoring of ZnO by means of heavy Al doping. *Phys. Rev. B* **1988**, *37*, 10244–10248, https://doi.org/10.1103/physrevb.37.10244.

11. Deng, H.; Fei, X.; Yang, Y.; Fan, J.; Yu, J.; Cheng, B.; Zhang, L. S-scheme heterojunction based on p-type $ZnMn_2O_4$ and n-type ZnO with improved photocatalytic CO_2 reduction activity. *Chem. Eng. J.* **2021**, *409*, 127377, https://doi.org/10.1016/j.cej.2020.127377.
12. Klingshirn, C. ZnO: Material, physics and applications. *ChemPhysChem* **2007**, *8*, 782–803.
13. Chen, D.; Wang, Z.; Ren, T.; Ding, H.; Yao, W.; Zong, R.; Zhu, Y. Influence of Defects on the photocatalytic activity of ZnO. *J. Phys. Chem. C* **2014**, *118*, 15300–15307, https://doi.org/10.1021/jp5033349.
14. Li, Q.; Zhai, G.; Xu, Y.; Odoom-Wubah, T.; Jia, L.; Huang, J.; Sun, D.; Li, Q. Diatomite supported Pt nanoparticles as efficient catalyst for benzene removal. *Ind. Eng. Chem. Res.* **2019**, *58*, 14008–14015, https://doi.org/10.1021/acs.iecr.9b02835.
15. Pookmanee, P.; Thippraphan, P.; Jansanthea, P.; Phanichphant, S. Characterization and adsorption efficiency of the natural and the modified diatomite via the low temperature hydrothermal route. *Adv. Mater. Res.* **2012**, *506*, 425–428, https://doi.org/10.4028/www.scientific.net/amr.506.425.
16. Chen, C.; Liu, P.; Lu, C. Synthesis and characterization of nano-sized ZnO powders by direct precipitation method. *Chem. Eng. J.* **2008**, *144*, 509–513, https://doi.org/10.1016/j.cej.2008.07.047.
17. Long, X.; Wang, C.; Wei, S.; Wang, T.; Jin, J.; Ma, J. Layered double hydroxide onto perovskite oxide-decorated ZnO nanorods for modulation of carrier transfer behavior in photoelectrochemical water oxidation. *ACS Appl. Mater. Interfaces* **2020**, *12*, 2452–2459, https://doi.org/10.1021/acsami.9b17965.
18. Ristic, M.; Music, S.; Ivanda, M.; Popović, S. Sol–gel synthesis and characterization of nanocrystalline ZnO powders. *J. Alloy. Compd.* **2005**, *397*, L1–L4, https://doi.org/10.1016/j.jallcom.2005.01.045.
19. Aksoy, S.; Caglar, Y.; Ilican, S.; Caglar, M. Sol–gel derived Li–Mg co-doped ZnO films: Preparation and characterization via XRD, XPS, FESEM. *J. Alloys Compd.* **2012**, *512*, 171–178.
20. Kaftelen, H.; Ocakoglu, K.; Thomann, R.; Tu, S.; Weber, S.; Erdem, E. EPR and photoluminescence spectroscopy studies on the defect structure of ZnO nanocrystals. *Phys. Rev. B* **2012**, *86*, https://doi.org/10.1103/physrevb.86.014113.
21. Kappers, L.; Gilliam, O.; Evans, S.; Halliburton, L.; Giles, N. EPR and optical study of oxygen and zinc vacancies in elec-tron-irradiated ZnO. *Nucl. Instrum. Methods Phys. Res. Sect. B Beam Interact. Mater. Atoms.* **2008**, *266*, 2953–2957.
22. Al-Gaashani, R.; Radiman, S.; Daud, A.; Tabet, N.; Al-Douri, Y. XPS and optical studies of different morphologies of ZnO nanostructures prepared by microwave methods. *Ceram. Int.* **2013**, *39*, 2283–2292, https://doi.org/10.1016/j.ceramint.2012.08.075.
23. Abdel-Wahab MS, Jilani A, Yahia I, Al-Ghamdi AA. Enhanced the photocatalytic activity of Ni-doped ZnO thin films: Morphological, optical and XPS analysis. *Superlattices Microstruct.* **2016**, *94*, 108–118.
24. Wu, L.; Zhou, Y.; Nie, W.; Song, L.; Chen, P. Synthesis of highly monodispersed teardrop-shaped core-shell. SiO_2/TiO_2 nanoparticles and their photocatalytic activities. *Appl. Surf. Sci.* **2015**, *351*, 320–326.
25. Yu, X.; Zhao, Z.; Zhang, J.; Guo, W.; Li, L.; Liu, H.; Wang, Z.L. One-step synthesis of ultrathin nanobelts-assembled urchin-like anatase TiO_2 nanostructures for highly efficient photocatalysis. *CrystEngComm* **2017**, *19*, 129–136, https://doi.org/10.1039/c6ce02241c.
26. Xu, H.-Q.; Hu, J.; Wang, D.; Li, Z.; Zhang, Q.; Luo, Y.; Yu, S.-H.; Jiang, H.-L. Visible-light photoreduction of CO_2 in a metal–organic framework: Boosting electron–hole separation via electron trap states. *J. Am. Chem. Soc.* **2015**, *137*, 13440–13443, https://doi.org/10.1021/jacs.5b08773.
27. Kang, Y.; Yang, Y.; Yin, L.-C.; Kang, X.; Wang, L.; Liu, G.; Cheng, H.-M. Selective breaking of hydrogen bonds of layered carbon nitride for visible light photocatalysis. *Adv. Mater.* **2016**, *28*, 6471–6477, https://doi.org/10.1002/adma.201601567.
28. Azarang, M.; Shuhaimi, A.; Yousefi, R.; Golsheikh, A.M.; Sookhakian, M. Synthesis and characterization of ZnO NPs/reduced graphene oxide nanocomposite prepared in gelatin medium as highly efficient photo-degradation of MB. *Ceram. Int.* **2014**, *40*, 10217–10221, https://doi.org/10.1016/j.ceramint.2014.02.109.
29. Neena, D.; Kondamareddy, K.K.; Bin, H.; Lu, D.; Kumar, P.; Dwivedi, R.K.; Pelenovich, V.; Zhao, X.-Z.; Gao, W.; Fu, D. Enhanced visible light photodegradation activity of RhB/MB from aqueous solution using nanosized novel Fe-Cd co-modified ZnO. *Sci. Rep.* **2018**, *8*, 1–12, https://doi.org/10.1038/s41598-018-29025-1.
30. Wang, Y.N.; Li, J.; Wang, Q. The performance of daylight photocatalytic activity towards degradation of MB by the flower-like and approximate flower-like complexes of graphene with ZnO and Cerium doped ZnO. *Optik* **2020**, *204*, 164131, https://doi.org/10.1016/j.ijleo.2019.164131.
31. Jeong, K.; Deshmukh, P.R.; Park, J.; Sohn, Y.; Shin, W.G. ZnO-TiO_2 core–shell nanowires: A sustainable photoanode for enhanced photoelectrochemical water splitting. *ACS Sustain. Chem. Eng.* **2018**, *6*, 6518–6526.